Contents lists available at ScienceDirect

Biosensors and Bioelectronics

journal homepage: http://ees.elsevier.com

Reliable and highly sensitive biosensor from suspended MoS_2 atomic layer on nano-gap electrodes

Nirul Masurkar [a], Naresh Kumar Thangavel [a], Sally Yurgelevic [b], Sundeep Varma [c], Gregory W. Auner [b], Leela Mohana Reddy Arava [a,*]

[a] Department of Mechanical Engineering, Wayne State University, Detroit, MI, 48202, USA
[b] Michael and Marian Ilitch Department of Surgery, School of Medicine, Wayne State University, Detroit, MI, 48202, USA
[c] Department of Electrical and Computer Engineering, Wayne State University, Detroit, MI, 48202, USA

ARTICLE INFO

Keywords
Biosensors
Field effect transistors
Escherichia coli
MoS_2
Nanogap

ABSTRACT

The uneven morphology and the trapped charges at the surface of the traditionally used supporting substrate-based 2D biosensors produces a scattering effect, which leads to a irregular signals from individually fabricated devices. Though suspended 2D channel material has the potential to overcome scattering effects from the substrates but achieving reliability and selectivity, have been limiting the using of this biosensor technology. Here, we have demonstrated nanogap electrodes fabrication by using the self-assembly technique, which provides suspension to the 2D-MoS_2. These nano-spacing electrodes not only give suspension but also provide robustness strength to the atomic layer, which remains freestanding after coating of the Hafnium oxide (HfO_2) as well as linkers and antibodies. For evaluating the electrical characteristics of suspended MoS_2 FET, gating potential was applied through an electrolyte on the suspended MoS_2 transistor. This helped in achieved a lower subthreshold swing 70 mV/dec and ON/OFF ratio 10^7. Later, pH detection was conducted at room temperature, which showed an impressive sensitivity of ~880 by changing 1 unit of pH. We have also successfully shown *Escherichia coli* (*E. coli*) bacteria sensing from the suspended MoS_2 transistor by functionalizing dielectric layer with *E. coli* antibodies. The reported biosensor has shown the ~9% of conductance changes with a lower concentration of *E. coli* (10 CFU/mL; colony-forming unit per mL) as well as maintain the constant sensitivity in three fabricated devices. The obtained enhancement in the sensitivity of devices and its effect on biomolecules detection can be extened to other biomolecules and this type of architecture has the potential to detect COVID-19 viruses based biomolecules.

1. Introduction

Due to their potential of providing continuous and real-time information, biosensors are prominent devices in the medical field and are garnering substantial interest in other domains such as forensic industries, national security, and ecological monitoring (Mehrotra and research, 2016). Specifically, electrochemical field-effect transistor (FET)-based biosensors have been recognized as one of the most promising candidates because of their compatibility with electronic devices, low power consumption, label-free detection of specific biomolecules, and low-cost mass production (Kim et al., 2016; Kuriyama and Kimura 1991; Suvarnaphaet and Pechprasarn 2017). In FET based biosensors, the charged biomolecules generate the electrostatic effect and bring the variation in the conductivity of the channel, which can be easily measured by transistor characteristics like source to drain current (Kaisti 2017; Sarkar et al., 2014a). To obtain better electrostatic effects from charged biomolecules, many semiconducting materials have been employed (Holzinger et al., 2014; Li et al., 2017; Zhu et al., 2012). Among the various materials, two-dimensional (2D) semiconducting materials holds great promise because of their tunable bandgap and a high surface to volume ratio that provides higher sensitivity for detection of biomolecules.

In the 2D domain, transition metal dichalcogenides (TMDs) like MoS_2 have gained much attention in the field of FET-biosensor due to their direct bandgap, biocompatibility, and high mobility (Kalantar-zadeh and Ou 2015b). Despite these merits, the performance and consistency of these atomic layers are easily affected by supporting substrate interaction (Chen et al., 2018). Such an interaction of supporting substrate with atomic layers of MoS_2 degrades the transport properties due to scattering, which implies that, interface control is vital for the performance and reliability of biosensor devices

* Corresponding author.
E-mail address: leela.arava@wayne.edu (L.M. Reddy Arava)

https://doi.org/10.1016/j.bios.2020.112724
Received 29 April 2020; Received in revised form 7 October 2020; Accepted 12 October 2020
Available online xxx
0956-5663/© 2020.

UNCORRECTED PROOF

(Du et al., 2008). For instance, the surface of silicon dioxide (SiO_2) substrate is highly disordered as well as chemically active due to the trapped atmospheric gases, chemical adsorbates, and unknown functional groups (Zhang et al., 2009). Therefore, transferring another layer of MoS_2 on the top of SiO_2 or any other insulating substrate cannot contribute to carrier charge transport distinctly, which leads to an unreliable output from every single device. In recent years, many efforts have been employed to enhance the quality of the substrate, such as placing an active layer interface by using Poly (methyl methacrylate) (PMMA) and polymer electrolytes [9]. These layers elude chemical bonding or surface roughness and improve carrier transport properties, but they cannot be employed in biosensor applications due to the difficulty in fabrication and reproducibility issues. The other approach is creating suspension of an atomic layer in between electrodes to enhance the carrier transport and remove scattering effect by wet etching of the SiO_2 layer underneath the monolayer MoS_2. Freestanding MoS_2 has shown better performance than the supporting on the SiO_2 substrate in terms of back gating electronic conduction (Jin et al., 2013). However, the existing SiO_2 requires hazardous chemical etchants such as hydrofluoric acid (HF), which is difficult to handle and affects the 2D film structure and purity (Zhang et al., 2017). Secondly, freestanding MoS_2 sags between the two electrodes because of the large spacing (~2 μm), which makes it impossible to coat dielectric layers such as hafnium oxide (HfO_2) and antibodies. Therefore, this structure impedes making top gate FET biosensors and allows only back gating. However, the back-gate FET requires more power (input gate voltage) to turn ON the device than the top gate, which hinders making a low power and highly sensitive biosensor. In FET based biosensor, the sensitivity is inversely proportional to the subthreshold swing (SS), which is defined as a change in the current with respect to dielectric surface potential ($SS = dV_{\text{gate}}/\log_{10} I_{\text{drain}}$; *dVgate* and *Idrain* are a change in gate potential and drain current respectively). Thus, back gate requires higher input voltage to turn on the device than the top gate, which reduces the sensitivity of detection (Sarkar et al. 2014a, 2014b).

Given the importance of reliability and sensitivity of FET based biosensor, in this work, chemical vapor deposition (CVD) grown MoS_2 is transferred by using novel dry stamping method on self-assembled photolithographically patterned nano-gaps to achieve suspension. Fabricated nanogap electrodes have 70–90 nm spacing, which provides mechanical strength to the MoS_2 monolayer and does not allow to sag between the two electrodes. This robustness in the monolayer film permits the coating of another thin dielectric layer as well as linkers/antibodies without interacting, supporting the substrate. HfO_2 as a dielectric material was considered, which is easily functionalized by a linker (3-Aminopropyl)triethoxysilane (APTES), glutaraldehyde, and *E. coli* antibodies to bring variation to the suspended 2D MoS_2 by targeting a charged *E. coli* bacteria. The suspended FET architecture lowered down the subthreshold swing (SS) to 70 mV/dec by terminating the scattering phenomenon and enhance the sensitivity of the pH as well as *E. coli* detection (Liao et al., 2018). Freestanding nature of 2D channel material i.e., MoS_2, retains its intrinsic properties and provides reliability and consistency in every single device.

2. Experimental section

2.1. CVD synthesis

Experimental procedures of CVD (In-house built) grown MoS_2 are as follows: quartz boat consists of MoO_3 powder, and SiO_2/Si pieces (top of the powder) were positioned in the middle of furnace whereas sulphur boat was placed at the upstream of lower temperature zone. In the typical process flow of CVD growth of MoS_2, Argon gas was passed for 20 min at 250 sccm to wash out all environmental gases and then ramp up the temperature till 750 °C in 15 min. Afterward, the temperature was maintained at 750 °C for 20 min. In this condition, sulphur starts evaporating and reduced MoO_3 to converts into metallic MoO_2. Further, more sulphurization of MoO_2 leads towards the triangular shape of MoS_2 flakes on the SiO_2/Si pieces.

2.2. Photolithography of nanogaps

In this process, the self-assembly technique was adapted to achieve nanogaps between the metal electrodes. Here, few parameters were optimized while fabrication such as lift-off resists thickness, rpm rate of spinning photoresist, baking, developing the photoresist, avoiding the residues during fabrication, and most importantly the optimization of thickness of metal electrode layer. The optical photolithography technique of patterning the substrate was done by coating the first positive photoresist (MICROPOSIT S1800) and expose (SUSS MicroTec Mask Aligner MA6) it for 80 mJ/cm^2 (flood exposure). Then another layer of photoresist 1811 is coated on the top and patterned with design chrome mask followed by evaporation of the Ti/Au/Cr (thickness is 10 nm/50 nm/80 nm). After patterning three metal layers Ti/Au/Cr, the wafer is kept for 12 Hrs. to control thermal oxidation of the chromium to achieve nanogap. Nano-spacing between electrodes rely on the rate of oxidation of the Cr layer, where temperature controls the rate of the oxidation. Therefore, it is essential to maintain the temperature as well as environmental gases of the wafer constant throughout the oxidation process. To achieve the proper pattern of the second layer, the thickness of the Ti/Au (second layer, whose thickness is 10 nm/50 nm) should not exceed more than 50% of chromium thickness. Liftoff the chromium as well as the second Au electrode is processed in chromium etchant solution (Chromium etchant, Sigma Aldrich).

2.3. Electrical characterization

Before transferring the 2D material, it was characterized by the current-voltage method. I–V curve between two electrodes was measured by the source meter (Keysight B2912A) to discern its electrical characteristics.

2.4. Transferring of 2D material and coating of the HfO_2

After achieving the optimum nanogap electrodes, triangular shape MoS_2 atomic layers was transferred on the top of the spacing by using a novel dry stamping method. This method provides proper placement of CVD grown MoS_2 in the desired area. Atomic layer deposition (ALD), University of Michigan, Ann Arbor (Veeco Fiji ALD), was performed to deposit 25 nm of the high dielectric layer.

2.5. Raman and AFM characterization

Prepared samples of MoS_2 are characterized by Raman Spectroscopy using 514 nm green (Nd-YaG) laser, whereas AFM (XE NSOM) mapping was performed by using a customized tip purchased from App Nano.

2.6. Functionalization of the HfO_2

3-Aminopropyltriethoxysilane (99%) (Sigma Aldrich), glutaraldehyde solution (50 wt% in H_2O, Bio Basic), *E. coli* antibodies (Rabbit polyclonal to *E. coli*, Abcam) was utilized for functionalization of the HfO_2. The suspended device was absorbed into APTES for 2 Hrs. in the ethanol/water mixture followed by the cleaning of the chip by

UNCORRECTED PROOF

ethanol and then blow-dried. Subsequently, APTES was functionalized on chip by immersing them in a glutaraldehyde solution for approximately 1 Hr. Afterward, *E. coli* antibodies were incubated to the suspended chip in 0.05 M PBS solution for 2 Hrs. at room temperature.

2.7. Bacteria growth

Bacterial specimens used in the study were prepared from culture plates. An isolated singer colony was added to 5 ml of media in a 14 ml culture tube. The culture tube was placed on a shaker in a 37 °C incubator and incubated overnight (18 h). The overnight culture was centrifuged at room temperature for 5 min at 3500 rpm. The supernatant was removed, and the bacteria pellet was re-suspended in 5 ml of filtered sterilized tap water. The bacteria were centrifuged, and the washing process was repeated once. After the final wash, filtered tap water was added to the bacteria pellet until the optical density (measured at a wavelength of 600 nm using a Spectro Max PLUS spectrophotometer) of the solution reached the desired value. After the optical density at 600 nm was measured for the stock solution, serial dilutions were employed.

3. Results and discussions

3.1. Suspended biosensor fabrications

Our approach for patterning the nanogap electrode uses a self-assembly photolithography technique, as shown in Fig. 1 (a). The metal lift-off method has been used for engraving the first electrode gold (Ti/Au) and chromium (Cr), the thickness of the Au was kept less than the Cr because it acts as a sacrificial layer as represented in Fig. 1(a) step I. After achieving the first electrode, the wafer was kept at ambient temperature for an overnight where Cr gets oxidized and forms a thin layer of Cr_xO_y. Due to the formation of Cr_xO_y, the overall volume of the Cr increases by a few nanometers and overhangs on the edges of the bottom electrode, as demonstrated in Fig. 1(a) step II. It is crucial to keep the wafer in a controlled environment to achieve uniform expansion of the Cr to avoid unevenness in the nanogap and connection between two electrodes (Fursina et al., 2008). In the next step, Au is deposited and patterned for the second electrode. However, enlargement of the Cr layer in a few nanometers protects the second electrode from meeting the first metal layer and creates the nanometer spacing, as shown in Fig. 1 (a) step III. At IV step, Cr was stripped out left behind two Au elec-

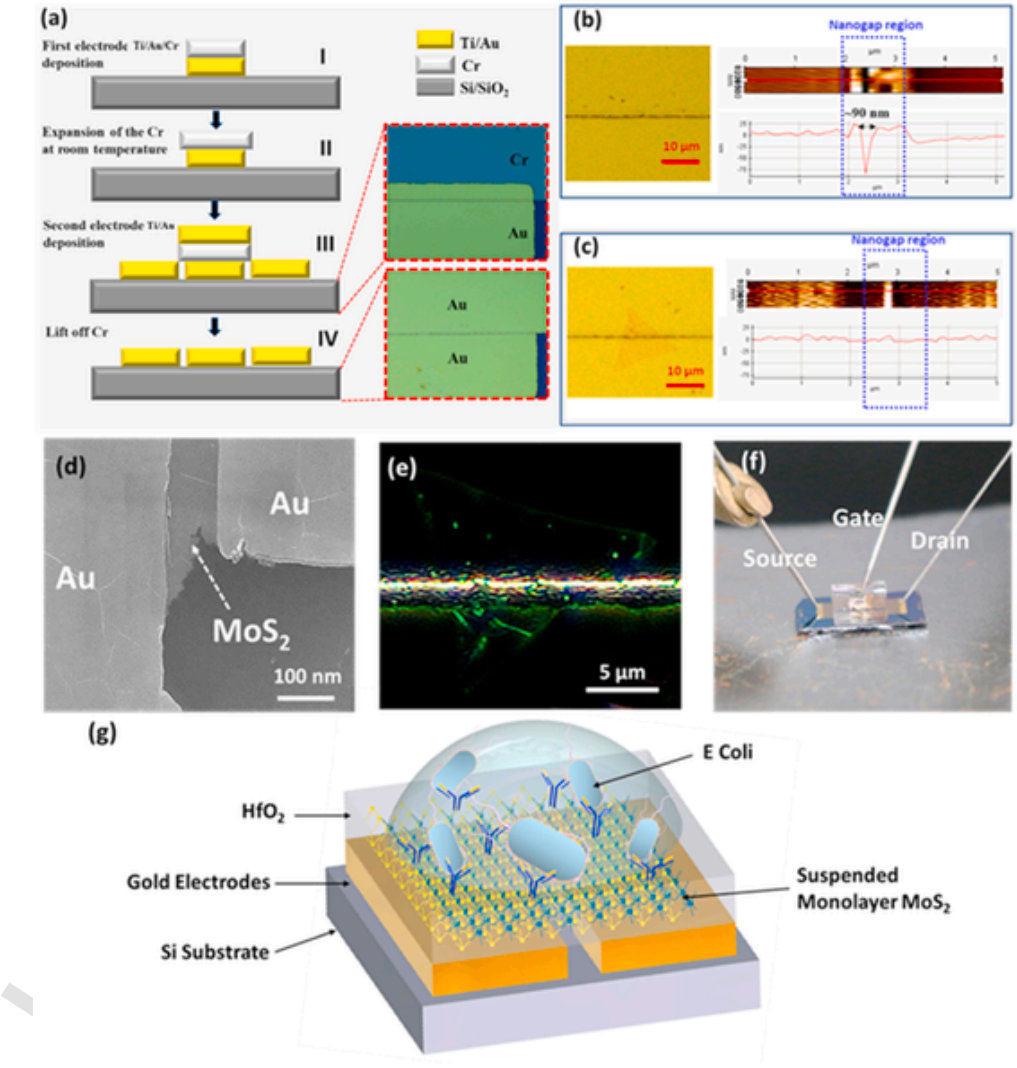

Fig. 1. Fabrication of suspended MoS_2 **FET**: (a) Schematic representation of the process flow to achieve nanogap electrodes. Optical image, AFM mapping, and line diagram of nanogaps (b) without MoS_2 (c) with MoS_2. (d) high magnification SEM image of MoS_2 on the top of nanogaps (e) Optical dark field image of MoS_2 triangle on the top nanogaps. (f) Image of biosensor device with Source, Drain, and Gate (Ag/AgCl electrode) connection (g) Schematic of Biosensor with *E. coli* and antibodies.

trodes, which are separated by few nanometers. In this self-assembly technique, the lateral resolution of the gap between two gold electrodes achieved nearly 70–90 nm at room temperature. The nanogap spacing between two electrodes is reproducible, constant throughout the wafer, and feasible for bulk fabrication due to the involvement of the wafer-scale lithography. To examine the fabricated electrode, which is not electrically connected, the voltage sweep has been performed, and the resulting current was monitored. This electrical characteristic demonstrated open circuit or short circuit between two nanogap electrodes (Supplementary Fig. 1). Throughout the wafer scale fabrication process of the nanogaps, there are several factors involves for achieving high yield such as chromium thickness, thermal oxidation, and thickness of the second layer Ti/Au. In our optimized process flow, the yield of the constant spacing was 70%–80% ($\pm$4 nm), which are mostly found in the center of the Silicon wafer.

For channel material in FET, CVD grown MoS_2 atomic crystals used in this work, which was characterized by using Raman spectroscopy and atomic force microscopy (AFM) (Supplementary Fig. 2). After achieving nanogap electrodes, a single atomic layer of MoS_2 flake was transferred on the top of nano spaced electrode by using a novel dry stamping method (Supplementary Fig. 3). The PMMA acts a sacrificial layer to transfer 2D material onto the nano gap electrode. After the transfer is done the PMMA is removed by placing the device in acetone bath, this will dissolve the PMMA without affecting 2D material transferred onto the nano gaps. This dry stamping method allows transferring a single crystalline MoS_2 triangle precisely on the top of nanogaps by using a micromanipulator. Nano-spacing between the electrode (90 nm) does not allow the MoS_2 membrane (0.65 nm) to touch the supporting substrate, and it is suspended in between the two electrodes. To confirm the free-standing nature of MoS_2, AFM imaging was performed on the nanogap region with and without MoS_2 to elucidate the suspension of the atomic layer on the electrodes. Fig. 1 (b) shows the optical image and AFM mapping with the line profile of the nanogap area without MoS_2 flake. AFM line profile of nanogap electrodes demonstrates the step height of 75 nm in between the two Au electrodes, which confirms the two metal layers are separated by nanometer spacing. Fig. 1(c) represents the optical image and AFM mapping of transferred MoS_2. AFM line profile of transferred MoS_2 on the top of nanogap indicates the flat line and no step height, which verify that the atomic membrane is suspended and is remarkably stiff as well as robust. This stiffness of the atomic layer confirms that it doesnot interacted with supporting substrates and possibly eliminates the scattering phenomena of the interface between the 2D material and the holder substrate. This mechanical strength provided by nano spacing does not allow the monolayer sagging between the electrodes, which permits depositing another layer, i.e., HfO_2 and biological receptor for selective sensing. To further validate the rigid suspension of the MoS_2 monolayer, a scanning electron microscope (SEM) and dark field image of the MoS_2 triangle on the top of the nanogaps were performed, as shown in Fig. 1 (d) & (e). These images clearly illustrate that the MoS_2 triangle does not sag in between the nanogap spacing; it is suspended and flat on the top of two Au electrodes.

After confirming the rigidness of the MoS_2, it is desirable to eliminate the density of defects by covering the bare channel material with insulating material and then functionalizing linkers and antibodies on the top of the insulator (Kalantar-zadeh and Ou 2015a; Sarkar et al., 2014a). If biomolecule directly functionalized on the semiconductor layer without insulation, it might attach to the metal electrodes and change the work function as well as the contact resistance, which leads to the reliability issue and bring the electrical variation in the sensor output. Therefore, the dielectric layer is essential to passivate the metal electrodes and eliminate direct contact with electrolyte or biomolecules. Therefore, a 25 nm HfO_2 dielectric layer is deposited on the top of the suspended device using atomic layer deposition (ALD). Afterward, macro fluidic storage is fabricated using Polydimethylsiloxane (PDMS) for encompassing electrolyte droplets, which is placed precisely on the top MoS_2 triangle covered with HfO_2. A reference electrode (Ag/AgCl) is used to apply bias through the electrolyte for stabilizing the process and better control of the operation under the biosensor regime, as shown in the optical image of Fig. 1 (f) (Sarkar and Banerjee 2012). Fig. 1 (g) represents the schematic structure of the suspended MoS_2 FET biosensor by selective detection of the *E. coli* bacteria.

3.2. Electrical characterization

The electrostatic effect of MoS_2 FET was investigated to compare the electrical performance of the supported and suspended devices. Fig. 2 represents the current-voltage (I–V) characteristics by applying different gate voltages (V_{BG}) of fabricated devices in a dry and wet environment. Fig. 2 (a) and (b) illustrates the I_D-V_{BG} curve of supported and free-standing MoS_2 at 100 mV bias voltage (V_{DS}), where supported channel length is 2 μm and suspended is ~90 nm. The suspended device represents excellent ON/OFF ratio 10^7 and threshold voltage (V_T) 3.9 V as compared to the supported one, which is equal to 10^6 and -9 V at room temperature. The improvement of the V_T, i.e., switching of the device at low voltage, is due to the elimination of the supporting substrate, which confines the electrons mean free path by scattering as well as from trapped charges on the surface (Masurkar et al., 2020). Fig. 2 (a') and (b') represents the I_D-V_{DS} characteristics at different V_{BG} (−10 V–30 V). In both cases, the V_{DS} varies from the 0 mV–100 mV, and the output current shows the linearity with the input voltage, which confirms that MoS_2 has ohmic contact with the Au/Ti contacts. Suspended FET displays better V_T and an ohmic contact with metal in back gate voltage characteristics. Still, due to the high power consumption, it is not feasible for use in the biosensor domain. Therefore, we have used a thin dielectric layer of the HfO_2 on the top of the channel and studied the ionic gating effect on the suspended MoS_2 channel, as shown in Fig. 2 (c) and (c'). Phosphate buffer solution as an electrolyte has been used for the ionic gating measurements by transporting a drop in macro fluidic storage. I_D-V_{LG} analysis of suspended ionic gating FET displayed impressive Subthreshold swing (SS) 70 mV/dec, which is near to ideal at room temperature as well as the mobility (13.5 $cm^2\ V^{-1}\ s^{-1}$) ON/OFF ratio (10^7) and V_T (− 0.29 V). The mobility of all three types of the devices are calculated and shown in the Supplementary Table S1 (Supplementary Fig. S4). Low SS, threshold voltage, high mobility and elimination of substrate scattering make these types of the FET structure more sensitive as well as consistency with better gate controllability in a wet environment.

3.3. pH sensing

After achieving excellent performance in the ionic gating effect, the suspended device was investigated by changing the pH of the electrolyte solution. The pH sensing strongly depends upon the proton (H^+) present in the electrolyte solution which is react with the OH group present on the HfO_2 surface and causes the protonation and deprotonation reaction, as shown in Fig. 3 (a) (Shadman et al., 2016). Depending upon the pH value of the electrolyte solution, the dielectric surface charge of the suspended FET varies, a lower pH value protonates the surface by generating OH_2^+ on the HfO_2 whereas the higher pH value deprotonates the surface by extracting H^+ (Ameri et al., 2015; Dinar et al., 2019). Fig. 3 (b) represents the drain current (I_D) (100 mV bias voltage) at different pH values (3, 5, 7, and 9) by changing the electrolyte gate voltage (V_{LG}). It is

UNCORRECTED PROOF

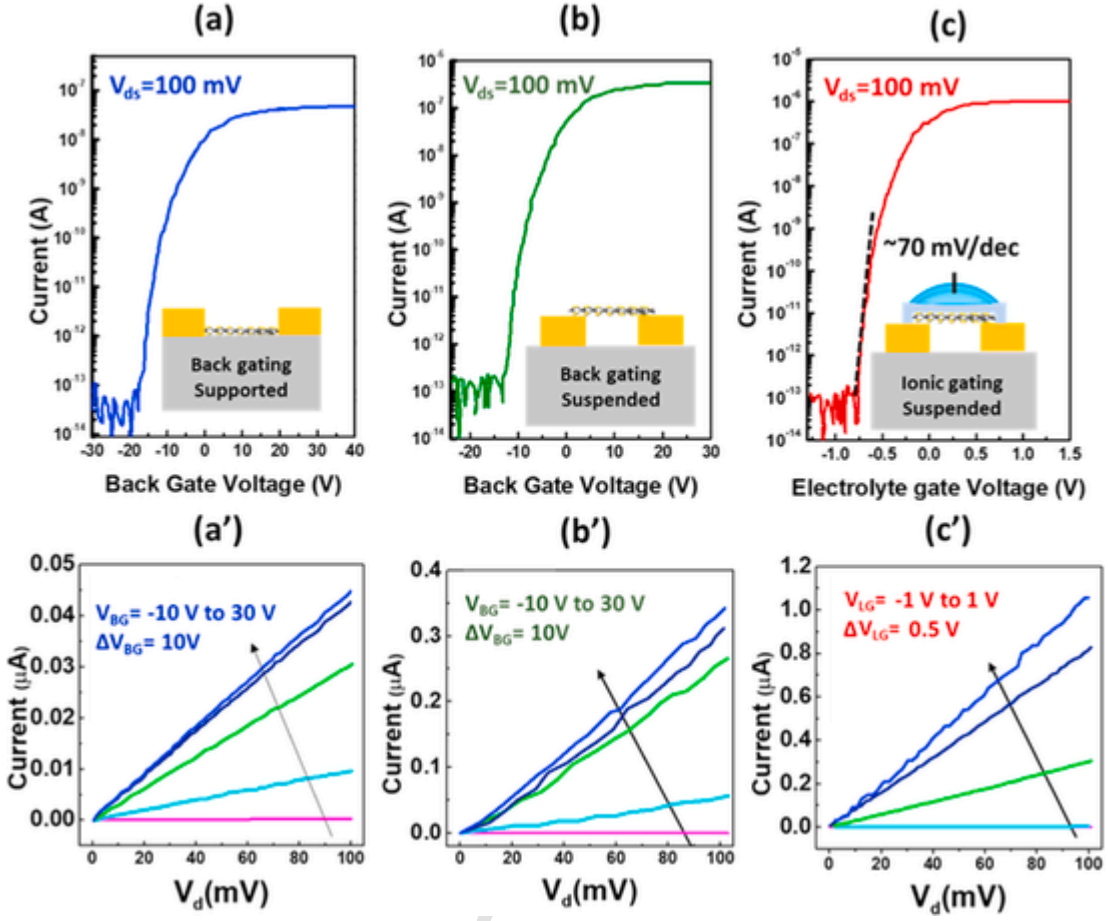

Fig. 2. Electrical characterization of suspended MoS_2 FET: Current-gate voltage curve at the constant bias 100 mV (a) back gating of supported MoS_2 (b) back gating of suspended MoS_2 with 90 nm channel length (c) Ionic gating of suspended MoS_2. Current-drain voltage characterization (a') Supported MoS_2 with back gating voltage from −10 V to 30 V (b') Suspended MoS_2 with back gating from −10 V to 30 V. (c') Suspended MoS_2 with ionic liquid gating from −1 V to 1V.

$$S_n = \frac{I_{pH1} - I_{pH2}}{I_{pH2}} \times 100 \quad (1)$$

found that the V_T of I_D-V_{LG} curves shifts to the positive side from low to high pH due to the negative charge developed on the dielectric surface. The change in ΔV_T found to be 59.1 mV/pH, which is satisfied the Nernst limit at room temperature, i.e., 59.3 mV/pH and agree with early studies of ion-sensitive field-effect transistor (ISFET) characterization on HfO_2 (Van Hal et al., 1995; Zafar et al., 2011). Therefore, HfO_2 does not require any functionalization for pH sensing as compared to the SiO_2, whose change in threshold voltage found to be 30–40 mV/pH (Bergveld and Physical 1996; Gao et al., 2009). Fig. 3 (c) represents the sensitivity of the pH at three different regions (Subthreshold, saturation, and linear), which is defined by the equation (1), where S_n is the sensitivity of pH, I_{pH1} and I_{pH2} are the transistor current measured from two different pH values (where pH1 > pH2).

The sensitivity at the subthreshold region was found to be much higher because the drain current is an exponential function of the gate voltage. In contrast, the saturation and linear parts are quadratic and linear with the change in gate potential. In a suspended device, the sensitivity at the subthreshold region was found to be ~876 from pH 5 to 6 and ~880 from pH 7 to 8 respectively, which is far better than the previous reports of MoS_2 FET biosensor on the supporting substrate (Sarkar et al., 2014b). The suspended MoS_2 FET possesses higher sensitivity than supported one because of the lower SS, where SS defined as the subthreshold swing. This equation elucidates that the change in subthreshold current by one decade is a function of the applied gate voltage, whereas the consistency in the sensitivity of the suspended device at two different ΔpH ranges is due to the elimination of the external scattering from the supporting substrate.

3.4. Bacteria sensing from suspended FET

Finally, suspended FETs are fabricated as described in the fabrication section to detect the biomolecules. To specifically detect the *E. coli* bacteria from the buffer solution (pH = 7.4), linkers were immobilized on the top of the HfO_2. For evaluating the bonding of the linkers with oxide surface, di-thiol and (3-Aminopropyl)triethoxysilane (APTES) have used, followed by glutaraldehyde treatment and antibodies immobilization (Gunda et al., 2014; Lee et al., 2006). From these two molecules, APTES has shown promising I_D-V_{LG} curve shifts while detecting bacteria as compared to the di-thiol (Supplementary Fig. 5). It is interesting to see that after the functionalization of the APTES/glutaraldehyde linkers on the surface of the HfO_2, there is a small shift of the I_D-V_{LG} curve as illustrated (Supplementary Fig. 6). The overall process flow of the linkers binding, antibodies immobilization on suspended MoS_2 FET through macro storage fluidic channel to detect *E. coli* as shown in the schematic of Fig. 4 (a) (Gunda et al., 2014; Wu et al., 2013). The I_D-V_{LG} transfer

UNCORRECTED

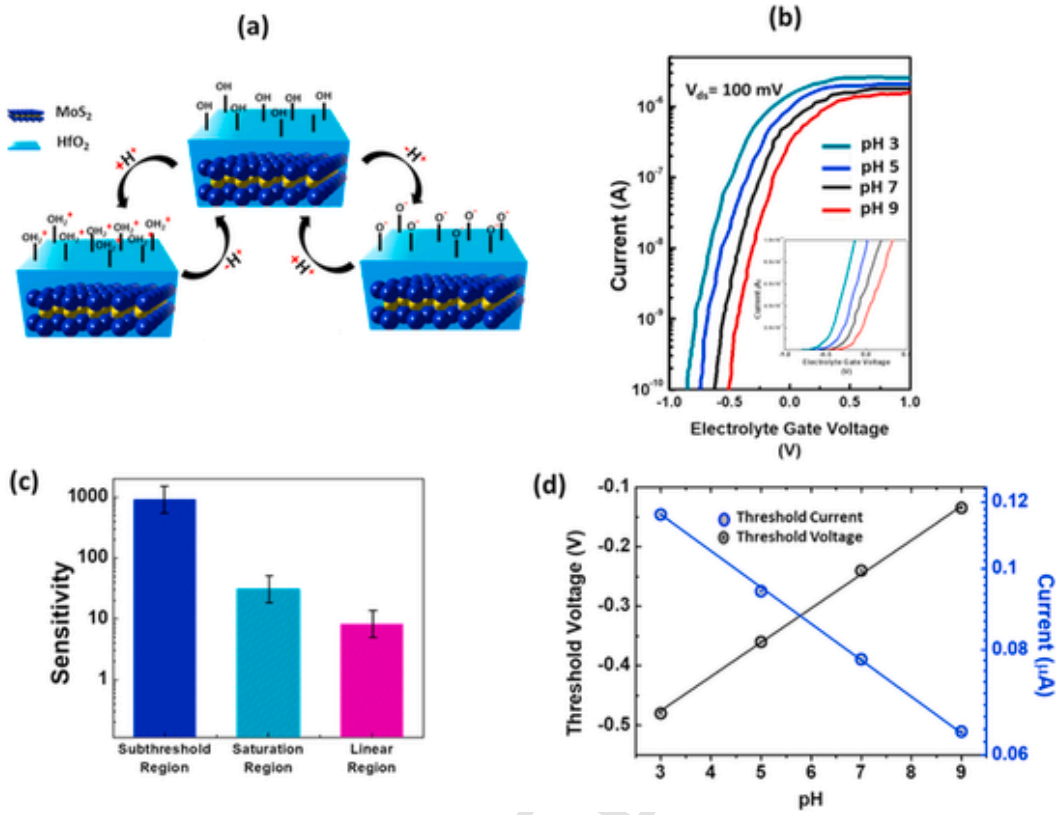

Fig. 3. pH detection of suspended MoS_2 **FET**: (a) Schematic of protonation and deprotonation on HfO_2 substrate. (b) I_D-V_{LG} curve of different pH concentration on the suspended MoS_2 (subset: Linear graph of I_D-V_{LG}). (c) Sensitivity of pH in subthreshold, saturation, and linear regions from pH 5 to pH 7. (d) experimental threshold voltage of suspended MoS_2 FET from pH 3 to pH 9 (Left-axis); experimental current corresponds to threshold voltage (Right-axis).

curve of the linkers, antibodies, PBS buffer solution, and the 100 CFU/mL of *E. coli* bacteria was performed, as demonstrated in Fig. 4 (b). It is essential to introduce a buffer solution again after antibodies immobilization to confirm there is no change of conductance (Cyan curve in Fig. 4 (b)). A shift found in the I_D-V_{LG} curve on the left side after incubation of 100 CFU/mL of *E. coli* (Magenta curve in Fig. 4 (b)).This illustrated that the current in the MoS_2 channel deteriorated due to the increment of hole concentration induced on the dielectric surface by highly negative charged bacteria wall (Huang et al., 2011).

After achieving considerable performance from the suspended MoS_2 FET device, different *E. coli* concentrations ranging from 0 to 10^3 CFU/mL were prepared and used for detection. The increase in the concentration of the bacteria leads to the decrement of the MoS_2 channel conductance. For buffer solution, I_D at (V_{LG} = 0V) is illustrated 0.3 μA, whereas 10 CFU/mL shows the current response 0.274 μA, the change in the conductance of freestanding MoS_2 was found to be ~9% with a low concentration of the bacteria. The change in conductance for 100 CFU/mL and 10^3 CFU/mL with buffer solution illustrated 18% and 25%, respectively, as shown in Fig. 4 (c). Another essential factor in the biosensor domain is selectivity, which attributes that other bacterial strain should not be attached with *E. coli* antibodies to achieve false signals. Therefore, *Pseudomonas aeruginosa* (*P. aeruginosa*) bacteria (100 CFU/mL) were considered to measure the I_D-V_{LG} signal by keeping V_{DS} = 100 mV. *P. aeruginosa* bacteria did not show any change in conductance as compared to the *E. coli* (100 CFU/mL), as shown in Fig. 4(d). Fig. 4 (e) illustrates the sensitivity of the biosensor, which is defined as shown in equ (2),

$$S_{n(cfu/ml)} = \frac{I_{\text{buffer}} - I_{n(CFU/mL)}}{I_{n(CFU/mL)}} \times 100 \quad (2)$$

where $S_{n(CFU/mL)}$ sensitivity, Buffer is a buffer solution current, $I_{n(CFU/mL)}$ is current after bacteria bind to the FET biosensor. It was found that the shift in I_D-V_{LG} is more in the subthreshold region as compared to saturation and linear regions. The sensitivity of the sensor in the subthreshold region achieved 83.3 for 100 CFU/mL of bacteria at −0.35 V. After obtaining higher sensitivity, the other most crucial factor in the 2D FET biosensor is the reliability in every fabricated sensor, which can be easily affected by external scattering from supporting substrate or the contact resistance from metal. In our case, we have maintained the constant work function between the electrode and the MoS_2 in every single device as well as eliminate the supporting substrate interaction, which attributes to the constant sensitivity in three suspended MoS_2 FET at the subthreshold region (100 CFU/mL and −0.35 V) as demonstrated in Fig. 4 (f).

The sensitivity presented in this report is found to be impressive as compare to the previous reports of biomolecule detection via 2D FET based technology. Graphene-based FET biosensor has shown the conductance change of 3.25% at 10 CFU/mL of *E. coli*, which is almost three times smaller than the presented value (9% at 10 CFU/mL) (Chang et al., 2013; Huang et al., 2011). The detection limits of the graphene are due to the zero band gap in nature, which leads to an increase in the off-state leakage current and the SS value (SS is inversely proportional to the sensitivity) (Schwierz 2010). On the other hand, FET based MoS_2 biosensor has shown promising sensitivity in biomolecule detection due to ~1.8 eV bandgap. However, the uneven morphology from the supporting substrate leads to an unreliable output from every single device due to different interface resistances caused majorly by trapped charges, chemical adsorbates,

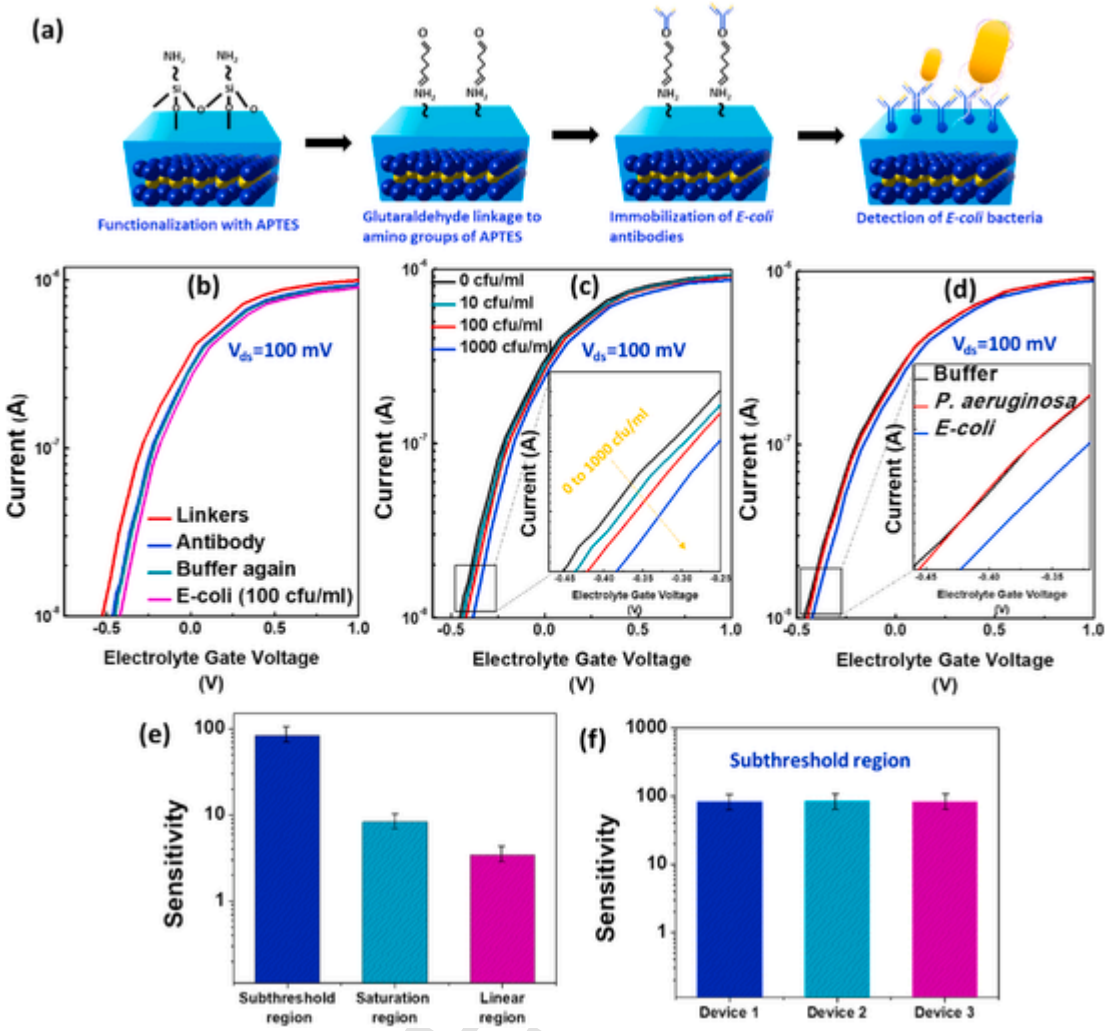

Fig. 4. *E. coli* bacteria detection on suspended MoS_2 **FET**: (a) Schematic diagram of self-assembly process for immobilization of *E. coli* bacteria on HfO_2 surface. (b) I_D-V_{LG} curve of SAM process at 100 mV bias; Functionalization of APTES (Red), immobilization of *E. coli* antibodies (Blue), buffer solution 0.01 M PBS solution of pH 7 (Cyan), and detection of *E. coli* bacteria of 100 CFU/mL (Magenta). (c) I_D-V_{LG} characterization of *E. coli* bacteria from 0 CFU/mL to 10^3 CFU/mL. (d) Comparison of I_D-V_{LG} characterization of *E. coli* and P. aeruginosa bacteria (100 CFU/mL) with PBS buffer solution. (e) Sensitivity measurement of *E. coli* bacteria at subthreshold, linear, and saturated regions. (f) Sensitivity comparison of three suspended MoS_2 FET devices by immobilizing the 100 CFU/mL E. *scoli* bacteria. (For interpretation of the references to colour in this figure legend, the reader is referred to the Web version of this article.)

and unknown functional groups (Jin et al., 2013; Kaushik et al., 2018). This is a significant barrier in proliferating this technology in biosensor industries. Therefore, elimination of the scattering effect in the proposed biosensor shows that the overall change of conductance in the 2D film is entirely due to the change in concentration of the biomolecule. Table S2 in Supporting Information represents a comparison of different 2D material based FET biosensor in terms of channel materials, detection limits, biomolecules, and sensitivity, whereas Table S3 in Supporting Information illustrates the comparison between different dimension and materials with respective their sensitivity, feasibility in bulk fabrication, and reliability. Due to these merits i.e., the involvement of the CVD method, direct transfer technique, and optical lithography open the new avenues for the bulk fabrication of suspended MoS_2 biosensor.

4. Conclusion

In summary, we provide an comprehensive approach for fabrication highly sensitive and reliable biosensor based on suspended MoS_2 FET to detect the pH as well as *E. coli* bacteria. CVD grown MoS_2 channel material was transferred on photolithographically patterned nano-gaps to achieve suspension and covered with Hafnium oxide (HfO_2) as a dielectric material to eliminate direct functionalization on the channel material. The proposed biosensor demonstrated the reliable and quantitative detection of pH and biomolecule by eliminating the scattering effect from the supporting substrate. A control experiment of pH sensing confirms that the high sensitivity (~880/pH) as well as the constant I_D-V_{LG} curve shift at different pH range (3–9). Suspended MoS_2 FET biosensor provides selective detection of the *E. coli* bacteria as low as 10 CFU/mL through changes in the conductance by 9% of MoS_2 channel at ultralow power (V_{DS} = 100 mV). This architecture can detect the low concentration of biomolecule because of the atomic layer as a channel material, and is scalable due to the involvement of optical photolithography, dry stamping, and CVD technique as well as reliable and reproducible due to the elimination of the supporting substrate. These merits of suspended MoS_2 FET biosensor makes it promising next-generation sensing device for on-spot detection of biomolecules and can be extened to COVID-19 viruses detection and bioelectronics applications.

UNDER

Declaration of competing interest

The authors declare that they have no known competing financial interests or personal relationships that could have appeared to influence the work reported in this paper.

Acknowledgments

This article was supported in part by the National Science Foundation under grant no 1751472 and ACS Petroleum Research Fund (ACS PRF: 57647-DNI10).

Appendix A. Supplementary data

Supplementary data to this article can be found online at https://doi.org/10.1016/j.bios.2020.112724.

References

Ameri, S., Singh, P., Sonkusale, S., 2015. Three Dimensional Monolayer Graphene Foam for Ultra-sensitive pH Sensing. 2015 Transducers-2015 18th International Conference on Solid-State Sensors, Actuators and Microsystems (TRANSDUCERS) pp. 1378–1380 IEEE.

Bergveld, P.J.S., Physical, A.A., 1996. The future of biosensors. 56 (1–2), 65–73.

Chang, J., Mao, S., Zhang, Y., Cui, S., Zhou, G., Wu, X., Yang, C.-H., Chen, J.J.N., 2013. Ultrasonic-assisted self-assembly of monolayer graphene oxide for rapid detection of Escherichia coli bacteria. 5 (9), 3620–3626.

Chen, H., Li, J., Chen, X., Zhang, D., Zhou, P.J.S.S., Technology, 2018. Dramatic switching behavior in suspended MoS2 field-effect transistors. 33 (2), 024001.

Dinar, A.M., Zain, A.M., Salehuddin, F.J., Engineering, C., 2019. Comprehensive identification of sensitive and stable ISFET sensing layer high-k gate based on ISFET/electrolyte models. 9 (2), 926.

Du, X., Skachko, I., Barker, A., Andrei, E.Y.J.N.n., 2008. Approaching ballistic transport in suspended graphene. 3 (8), 491.

Fursina, A., Lee, S., Sofin, R., Shvets, I., Natelson, D.J.A.P.L., 2008. Nanogaps with very large aspect ratios for electrical measurements. 92 (11), 113102.

Gao, X.P., Zheng, G., Lieber, C.M.J.N.l., 2009. Subthreshold regime has the optimal sensitivity for nanowire FET biosensors. 10 (2), 547–552.

Gunda, N.S.K., Singh, M., Norman, L., Kaur, K., Mitra, S.K., 2014. Optimization and characterization of biomolecule immobilization on silicon substrates using (3-aminopropyl) triethoxysilane. APTES) and glutaraldehyde linker 305, 522–530.

Holzinger, M., Le Goff, A., Cosnier, S.J.F.i.c., 2014. Nanomaterials for biosensing applications: a review. 2, 63.

Huang, Y., Dong, X., Liu, Y., Li, L.-J., Chen, P.J., 2011. Graphene-based biosensors for detection of bacteria and their metabolic activities. 21 (33), 12358–12362.

Jin, T., Kang, J., Su Kim, E., Lee, S., Lee, C., 2013. Suspended single-layer MoS2 devices. J. Appl. Phys. 114 (16), 164509.

Kaisti, M., 2017. Detection principles of biological and chemical FET sensors. Biosens. Bioelectron. 98, 437–448.

Kalantar-zadeh, K., Ou, J.Z., 2015a. Biosensors based on two-dimensional MoS2. ACS Sens. 1 (1), 5–16.

Kalantar-zadeh, K., Ou, J.Z.J.A.S., 2015b. Biosensors based on two-dimensional MoS2. 1 (1), 5–16.

Kaushik, N., Ghosh, S., Lodha, S., 2018. Low-frequency noise in supported and suspended MoS 2 transistors. IEEE Trans. Electron. Dev. 65 (10), 4135–4140.

Kim, S.K., Bhatia, R., Kim, T.-H., Seol, D., Kim, J.H., Kim, H., Seung, W., Kim, Y., Lee, Y.H., Kim, S.-W.J.N.E., 2016. Directional dependent piezoelectric effect in CVD grown monolayer MoS2 for flexible piezoelectric nanogenerators. 22, 483–489.

Kuriyama, T., Kimura, J., 1991. FET-based biosensors. Bioproc. Technol. 15, 139–162.

Lee, L.M., Heimark, R.L., Baygents, J.C., Zohar, Y.J.N., 2006. Self-aligned immobilization of proteins utilizing PEG patterns 17 (4), S29.

Li, X., Shan, J., Zhang, W., Su, S., Yuwen, L., Wang, L.J.S., 2017. Recent advances in synthesis and biomedical applications of two-dimensional transition metal dichalcogenide nanosheets. 13 (5), 1602660.

Liao, W., Wei, W., Tong, Y., Chim, W.K., Zhu, C.J.A.a.m., interfaces, 2018. Low-frequency noise in layered ReS2 field effect transistors on HFO2 and its application for pH sensing. 10 (8), 7248–7255.

Masurkar, N., Varma, S., Mohana Reddy Arava, L., 2020. Supported and suspended 2D material-based FET biosensors. Electrochemistry 1 (3), 260–277.

Mehrotra, P.J., research, c., 2016. Biosensors and their applications–A review. 6 (2), 153–159.

Sarkar, D., Banerjee, K.J.A.P.L., 2012. Proposal for tunnel-field-effect-transistor as ultra-sensitive and label-free biosensors. 100 (14), 143108.

Sarkar, D., Liu, W., Xie, X., Anselmo, A.C., Mitragotri, S., Banerjee, K., 2014a. MoS2 field-effect transistor for next-generation label-free biosensors. ACS Nano 8 (4), 3992–4003.

Sarkar, D., Liu, W., Xie, X., Anselmo, A.C., Mitragotri, S., Banerjee, K.J.A.n., 2014b. MoS2 field-effect transistor for next-generation label-free biosensors 8 (4), 3992–4003.

Schwierz, F.J.N.n., 2010. Graphene transistors 5 (7), 487.

Shadman, A., Rahman, E., Khosru, Q.D.J.S., Research, B.-S., 2016. Monolayer MoS2 and WSe2 double gate field effect transistor as super nernst pH sensor and nanobiosensor. 11, 45–51.

Suvarnaphaet, P., Pechprasarn, S.J.S., 2017. Graphene-based materials for biosensors: a review. 17 (10), 2161.

Van Hal, R., Eijkel, J.C., Bergveld, P.J.S., Chemical, A.B., 1995. A novel description of ISFET sensitivity with the buffer capacity and double-layer capacitance as key parameters. 24 (1–3), 201–205.

Wu, S.-M., Chen, J., Ai, X.-X., Yan, Z.-Y.J., analysis, b., 2013. Detection of Escherichia coli in drugs with antibody conjugated quantum dots as immunofluorescence probes. 78, 9–13.

Zafar, S., D'Emic, C., Afzali, A., Fletcher, B., Zhu, Y., Ning, T.J.N., 2011. Optimization of pH sensing using silicon nanowire field effect transistors with HfO2 as the sensing surface. 22 (40), 405501.

Zhang, F., Erb, C., Runkle, L., Zhang, X., Alem, N., 2017. Etchant-free transfer of 2D nanostructures. Nanotechnology 29 (2), 025602.

Zhang, Y., Brar, V.W., Girit, C., Zettl, A., Crommie, M.F., 2009. Origin of spatial charge inhomogeneity in graphene. Nat. Phys. 5 (10), 722–726.

Zhu, Z., Garcia-Gancedo, L., Flewitt, A.J., Xie, H., Moussy, F., Milne, W.I.J.S., 2012. A critical review of glucose biosensors based on carbon nanomaterials. carbon nanotubes and graphene 12 (5), 5996–6022.

UNCORRECTED PROOF